

Received November 13, 2020, accepted November 30, 2020, date of publication December 4, 2020, date of current version December 17, 2020.

Digital Object Identifier 10.1109/ACCESS.2020.3042571

Frequency Properties of an Air-Cored Coil and Application to Conductivity Measurement

WEIYING CHENG 

NDE Center, Japan Power Engineering and Inspection Corporation, Yokohama 230-0044, Japan
Department of Quantum Science and Energy Engineering, Tohoku University, Sendai 980-8579, Japan
e-mail: cheng-weiyang@japeic.or.jp

This work was supported in part by the Japan Society for the Promotion of Science (JSPS) through Grants-in-Aid for Scientific Research (KAKENHI) under Grant JP20K05000.

ABSTRACT This study investigated the frequency properties of an air-cored coil and applied it to inspect conductivity change. Theoretical analysis and experimental study showed that what we measured is not the coil's own resistance and inductance but the equivalent ones which change with frequency. Case studies on conductivity measurement using a coil probe showed that we can greatly enhance measurement sensitivity by making the best of the coil's frequency properties. By utilizing the coil at frequencies that the coil's resistance and inductance are 'frequency-invariant', we were able to detect conductivity change with high sensitivity on the basis of 'same product of conductivity and frequency, $\omega\sigma$ (product of angular frequency and conductivity), same impedance' principle. The study also showed that we can use the coil's resonant properties, e.g., resonant frequency, resistance at resonant, to sense conductivity change, regardless of change on thickness. A slight variation of conductivity could be perceived by fine frequency adjustment. The results strongly suggest using a coil in accordance with its frequency characteristics.

INDEX TERMS Conductivity measurement, coil, eddy currents, frequency response, resonance.


I. INTRODUCTION

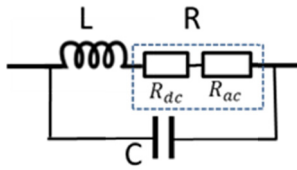
In most eddy current testing (ECT) studies, the coil used to induce eddy currents is ideally considered as an inductor of zero resistance, zero capacitance and constant inductance; eddy currents in the test object but not in the coil are analyzed [1]–[10]. Most actual ECT coils, however, are wound up with resistive copper wires and driven by alternating currents (AC) [1], [11]. The resistance and inductance of the coil change with frequency due to the eddy current effects in the windings. There is also stray capacitance between the windings; the coil may resonate at its self-resonant frequency (SRF). In conventional ECT, the coil generally operates far below its SRF; the resistance and inductance are considered to be frequency-invariant, the capacitance is neglected; a conventional ECT coil is generally modelled with a resistor and an inductor connected in series [1], [11].

In recent decades, the applicability of ECT is expanding, together with widening of operating frequency band. For instance, high frequency ECT has been introduced to inspect composite materials with low electrical conductivity [12]–[15]; extremely low frequency ECT has

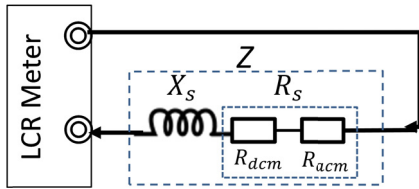
been applied to detect deeply buried defects [16]–[18]. Along with the development of high frequency and low frequency ECT probes, the conventional ECT probe coils are explored anew to 'unconventional' frequency ranges. Nevertheless, a profound understanding of a probe coil's frequency characteristics is essential.

Numerous investigations showed that electrical conductivities of iron and steel materials change in the process of degradations, such as creep, thermal aging, residual stress, and irradiation degradation [19]–[24]. Conductivity measurement, as a means of material characterization, has been extensively studied [5]–[8], [20]–[24]. The conductivity of bulk material is generally measured by applying direct current (DC) to a cut-off sample [2], [30] with uniform cross section over a particular length. The conductivity can be determined by measuring the potential drop and the current flowing through. This so called four-point method is direct and effective, however, the destructive 'cut off' is not acceptable for field inspection. The nondestructive measurement based on the ECT principle is an alternative solution [5]–[8], [20]–[24]. Instead of measuring the conductivity itself, the ECT method is particularly appropriate for detecting conductivity change. Nevertheless, the ECT signals are affected by probe setup, the test object's structural dimension and etc.

The associate editor coordinating the review of this manuscript and approving it for publication was Xiaokang Yin .



(a) Lumped element circuit model of a real coil.



(b) Quantities measured by an LCR meter in series mode.

FIGURE 1. Lumped element circuit model of an air-cored coil and the signals measured by an LCR meter.

The sensitivity of ECT measurement has yet to be improved. The objective of ECT conductivity measurement for material characterization is to detect conductivity change with high sensitivity independently of the test object’s structural dimension. Fulfilling the objective requires an appropriate ECT probe and proper measurement condition, which in turn significantly relies on the understanding of the probe’s frequency properties.

In this study, we investigated an air-cored coil’s frequency responses theoretically and experimentally, and established two methods to measure conductivity change in accordance with the frequency properties. Thereby, the conductivity change was sensitively detected by using the coil in its frequency-invariant range; the conductivity change was also detected regardless of a test object’s thickness using the coil’s resonant properties. The probe coil’s conductivity measurement ability, e.g., measuring range of conductivity and sensitivity, were also discussed.

II. FREQUENCY CHARACTERISTICS OF AN AIR-CORED COIL

First of all, we theoretically analyzed an air-cored coil’s frequency characteristics. The assumed N_c turn coil’s outer and inner radii are respectively r_{out} and r_{in} .

A. MODELING OF AN AIR-CORED COIL

Fig. 1(a) shows the air-cored coil’s lumped-element model: a resistor R and an inductor L connected in series, with a capacitor C in parallel. The resistance R consists of frequency-invariant resistance to DC current, R_{dc} , and increased resistance R_{ac} when AC currents flow through. R_{ac} changes with frequency. The coil’s total resistance, which is the sum of R_{dc} and R_{ac} , is frequency dependent accordingly,

$$R(\omega) = R_{dc} + R_{ac}(\omega), \quad (1)$$

where ω is the angular frequency. Hereafter, the description of frequency dependence, (ω) , is omitted for simplification.

The admittance in terms of lumped parameters is

$$Y = \frac{1}{R + j\omega L} + j\omega C,$$

where $R = R_{dc} + R_{ac}$. The impedance is

$$Z = \frac{1}{Y} = \frac{R + j\omega(L - \omega^2 L^2 C - CR^2)}{(1 - \omega^2 LC)^2 + (\omega CR)^2} = R_{eq} + jX_{eq} \quad (2)$$

that

$$R_{eq} = \frac{R}{(1 - \omega^2 LC)^2 + (\omega CR)^2} = R_{eq_dc} + R_{eq_ac}, \quad (3)$$

$$X_{eq} = \frac{\omega(L - \omega^2 L^2 C - CR^2)}{(1 - \omega^2 LC)^2 + (\omega CR)^2}. \quad (4)$$

R_{eq} and X_{eq} are the equivalent resistance and reactance. Equation (3) indicates that R_{eq} consists of frequency-invariant R_{eq_dc} and frequency-varying R_{eq_ac} . When $\omega = 0$, $R_{eq} = R_{eq_dc}$. R_{eq} is always larger than 0; the sign of X_{eq} , however, changes with $L - \omega^2 L^2 C - CR^2$. In other words, the coil may be inductive or capacitive, depending on frequency. The coil is inductive when $L - \omega^2 L^2 C - CR^2 > 0$, the equivalent inductance L_{eq} can be calculated by

$$L_{eq} = \frac{X_{eq}}{\omega} = \frac{(L - \omega^2 L^2 C - CR^2)}{(1 - \omega^2 LC)^2 + (\omega CR)^2}. \quad (5)$$

When $L - \omega^2 L^2 C - CR^2 = 0$, $X_{eq} = 0$, the coil is at resonant. The resonant frequency ω_r is

$$\omega_r = \frac{1}{\sqrt{LC}} \sqrt{1 - \frac{CR^2}{L}}, \quad (6)$$

and the impedance is reduced to the resistance at resonant, R_r ,

$$\begin{aligned} Z_r = R_r &= \frac{R}{(1 - \omega_r^2 LC)^2 + (\omega_r CR)^2} = \frac{R}{(\frac{CR^2}{L})^2 + (\omega_r CR)^2} \\ &= \frac{L}{CR}. \end{aligned} \quad (7)$$

Denoting $\omega_0 = \frac{1}{\sqrt{LC}}$ as the resonant frequency of a zero-resistance ideal coil, the resonant frequency of an actual coil is expressed in terms of ω_0 as

$$\omega_r = \omega_0 \sqrt{1 - \frac{CR^2}{L}} = \omega_0 \sqrt{1 - \frac{R}{R_r}}. \quad (8)$$

Equation (8) indicates that resonance occurs only when $\frac{CR^2}{L} < 1$, that is, $R < \sqrt{\frac{L}{C}}$. Equation (8) also shows that the resonant frequency of an actual coil is lower than that of an ideal coil, $\omega_r < \omega_0$; the resistance at resonance is larger than the resistance at other frequencies, $R_r > R$.

As can be seen from Fig. 1 and (2)-(5), what we measure are not the coil’s own resistance and inductance but the equivalent ones. The change of equivalent impedance with frequency attributes not only to the eddy current effects upon each lumped element (R , L and C) but also the synthetic actions of R , ωL and ωC . The equivalent resistance and

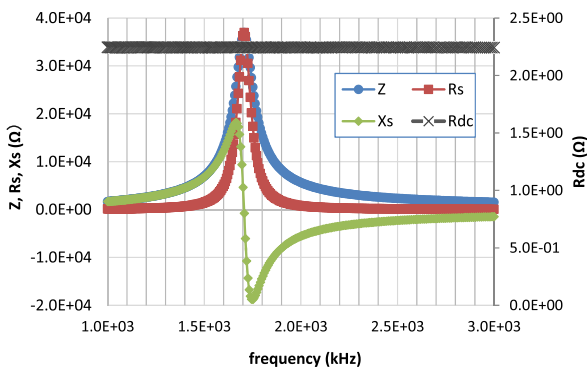


FIGURE 2. Frequency responses of the coil (from 1000kHz to 3000kHz).

inductance might be approximately equal to the coil’s own when the effect of C is negligible, but might be quite different otherwise. It is vital to understand the difference between the equivalent resistance and inductance and those of the coil itself.

B. MEASUREMENT OF THE FREQUENCY RESPONSE OF THE AIR-CORED COIL

Nevertheless, calculation of the frequency responses (R , L and C) of an actual multi-winding air-cored coil remains very challenging. In this study, we investigated a tightly wound air-cored coil’s frequency properties by measurement and clarified the signals by means of simplified qualitative analysis.

The air-cored coil used in this study is wound up with a 0.24mm diameter copper wire. The 85-turn coil’s inner and outer radii are respectively 8mm and 10mm, the thickness is 3mm. The coil was driven by constant AC current using an LCR meter (HIOKI IM3536 LCR Meter [28]) at frequencies from 5Hz to 3MHz. The LCR meter was set to series mode that the impedance Z , DC resistance R_{dc} , resistance R_s , and reactance X_s at each frequency can be measured directly (Fig. 1(b), the subscript ‘s’ stands for series mode, and the subscript ‘m’ for ‘measurement’). It can be seen from Fig. 1(b) that R_s , X_s and R_{dc} are respectively in correspondence to R_{eq} , X_{eq} and R_{dc} in the equivalent model.

Because of the limits on the LCR meter [28], the coil’s low frequency and high frequency responses were measured separately. At low frequencies that the coil is of low impedance, the driven current (in constant current mode) was set to a relatively large value (10mA) so as to get adequate voltage drop. Around resonant frequencies, however, the coil is of large impedance, the driven current was set to a smaller value (0.03mA) so that the voltage across the coil does not exceed the LCR meter’s upper limit on voltage (1.0V).

Fig. 2 shows the measured quantities at frequencies from 1MHz to 3MHz. As stated in the previous subsection A, the resistance to DC current, R_{dc} , is frequency-invariant, whereas the impedance Z and resistance R_s change with

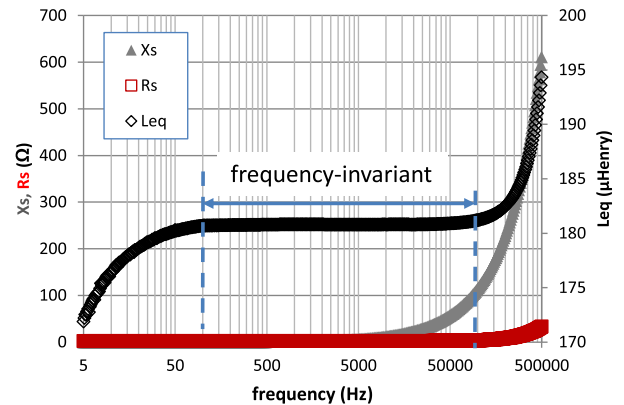


FIGURE 3. Frequency responses of the coil (from 5Hz to 500kHz).

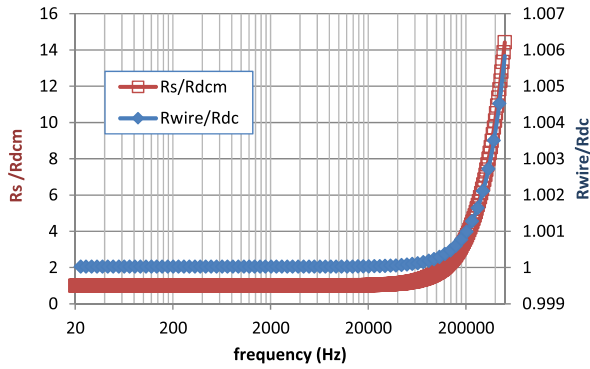
frequency. The Z and R_s reach maxima, whereas the reactance X_s drops to 0 at 1.648MHz. Obviously, 1.648MHz is the coil’s self-resonant frequency. The coil is inductive below 1.648MHz and capacitive above it.

Because a coil generally works far below its SRF in conventional ECT, the coil’s frequency responses at frequencies from 5Hz to 500kHz are separately plotted in Fig. 3, along with the equivalent inductance L_{eq} calculated by X_s/ω . It can be seen both R_s and X_s increase slowly with frequency up to about 80kHz, following by speed-up increment at frequencies above 80kHz. The equivalent inductance L_{eq} rises from 5Hz to 80Hz, keeps almost unchanged from 80Hz to 80kHz, and goes upward sharply from 80kHz to 500kHz. The L_{eq} is a result of the synthetic effect of resistance, inductance and capacitance. At frequencies from 5Hz to 80Hz, $|1/j\omega C|$ and $|j\omega L|$ are of comparable value, the equivalent L_{eq} is smaller than L . From 80Hz to 80kHz, the capacitor C in parallel can be neglected because $|1/j\omega C| \gg |j\omega L|$, the equivalent inductance and resistance are almost equal to the coil’s own. In this frequency range, the skin depth, which is a measure of the alternating current’s distribution near the surface of a conductor, is much larger than the wire’s radius, the alternating current distributes over the wire’s cross section with very low ‘uneven’ level. As a result, the coil’s own R and L change slightly with frequency. Apparently, this is the intended frequency band for conventional ECT. When the frequency increases further from 80kHz to 500kHz, the creep up of eddy current effects, together with the synthetic effect of resistance, inductance and capacitance, lead to rapid increase of R_{eq} and L_{eq} with frequency.

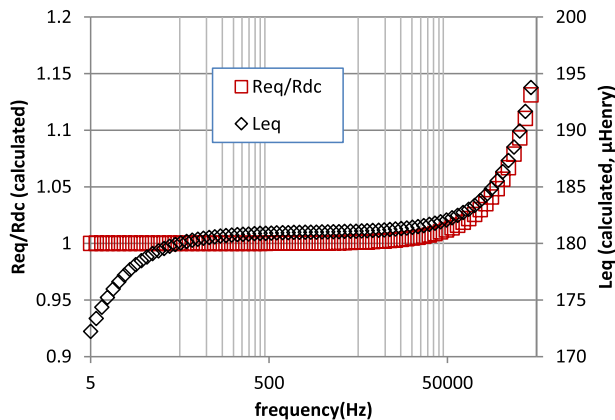
Hereafter is a numerical example to elucidate the change of resistance and inductance with frequency.

C. QUALITATIVE ANALYSIS OF THE COIL’S FREQUENCY RESPONSES

The winding wire is of radius a , permeability μ and electrical conductivity σ . The length of the N_c turn coil of outer radius r_{out} and inner radius r_{in} is $l = N_c * \pi (r_{out} + r_{in})$. The impedance of a straight conducting wire carrying alternating current of angular frequency ω was calculated by the



(a). Change of resistance ratios, R_s/R_{dcm} and R_{wire}/R_{dc} , with frequency.



(b). Equivalent inductance and resistance calculated by (4) and (5).

FIGURE 4. Comparison of calculated and measurement quantities.

following formula [25]

$$Z_{wire} = -j \frac{\omega \mu J_0(ka)}{2\pi ka J_1(ka)} = \frac{1}{2} R_{dc} ka \frac{J_0(ka)}{J_1(ka)}, \quad (9)$$

where j is the complex unit, $ka = \frac{a(1-j)}{\delta}$ and $\delta = \sqrt{\frac{2}{\omega \mu \sigma}}$ is the skin depth. J_0 is the 1st kind Bessel function of 0 order, and J_1 is the 1st kind Bessel function of 1st order. The resistance of the wire to DC current, R_{dc} , was approximately calculated by $R_{dc} = \frac{l}{\sigma \pi a^2}$. The resistance of the wire is equivalent to the real part of the impedance, $R_{wire} = \text{Re}(Z_{wire})$. The ratio of R_{wire} to R_{dc} is

$$R_{wire}/R_{dc} = \text{Re} \left[\frac{1}{2} ka \frac{J_0(ka)}{J_1(ka)} \right]. \quad (10)$$

We calculated the R_{wire}/R_{dc} by setting the conductivity and magnetic permeability of the copper wire as 58.5MS/m and $\mu_0 (= 4\pi \times 10^{-7} \frac{H}{m})$ and substituting the dimensional parameters, $N_c = 85$, $r_{out} = 10\text{mm}$, $r_{in} = 8\text{mm}$, $a = 0.12\text{mm}$, into (10). Fig. 4(a) shows the calculated R_{wire}/R_{dc} of the straight wire (including 2×30 cm long cable), along with the R_s/R_{dcm} obtained from measurement. Both the calculated quantity (R_{wire}/R_{dc}) and the measurement quantity

(R_s/R_{dcm}) are approximately equal to 1.0 at frequencies below 20kHz, and increase steadily at higher frequencies. However, the grow rate of R_{wire}/R_{dc} is much smaller than that of R_s/R_{dcm} . Because at 200kHz the skin depth of the copper wire, 0.26mm, is almost twice of the wire's radius, the increment of resistance due to skin effect is insignificant. By the way, the proximity effect, which describes the change of current distribution because of alternating magnetic field in adjacent conductors, between adjacent wires is generally less significant than the skin effect of the conductor itself. It is expected that even taking into account both the skin and proximity effects, the increment of resistance due to eddy current effects is not remarkable, the ratio of the coil's total resistance to DC resistance is just slightly larger than 1.0 at frequencies below 200kHz. On the assumption that the proximity effect affects the resistance similar to that of the skin effect, we substituted $R = R_{dc} \cdot (\frac{R_{wire}}{R_{dc}})^2$ into (3) to calculate the equivalent resistance. The squared $\frac{R_{wire}}{R_{dc}}$ is an approximation of resistance increment resulting from skin effect and proximity effect.

The self-inductance of the coil was calculated using the Wheeler's formula [26]. The calculated value ($182.5\mu H$) is almost equal to the measured value (about $181\mu H$ at frequencies from 80Hz to 80kHz, as shown in Fig. 3(b)). Therefore, we set the inductance to DC current, L_{dc} , to be $181.0\mu H$, and assumed that the self-inductance changes with frequency in a manner similar to resistance, and thereby substituted $L = L_{dc} \cdot (\frac{R_{wire}}{R_{dc}})^2$ into (5).

The capacitance C is also needed to calculate the equivalent resistance and inductance. There are few researches on a winding coil's stray capacitance. Herein we investigate the capacitance between two closely spaced turns of the coil in a qualitative way. The capacitance is defined as the ratio of charges (Q) accumulated in each turn to the potential difference (U) between the two turns, $C_{turn} = \frac{Q}{U}$. Because the coil was driven by AC current $i(t) = \text{Re}(Ie^{-j\omega t})$ that I is a constant, the charge $Q = \int i(t)dt$ is proportional to $1/\omega$. By the way, because the wire's impedance changes little with frequency, the potential difference $\dot{U}(= ZI)$ across the two adjacent turns changes little neither. As a result, C_{turn} is approximately proportional to $1/\omega$. In the calculation of equivalent inductance and resistance at frequencies from 5Hz to 500kHz, we substituted C with

$$C = C_0 \times \text{logspace}(a, b, n), \quad (11)$$

where logspace generates logarithmically spaced vector in MATLAB [26]. The argument a defines the first bound of the interval over which logspace generates points, and b is the second bound, n is the number of points. Herein, $C_0 = 2.1\mu F$, $a = 0$, $b = -4.75$, $n = 80$. That is, the stray capacitance is assumed to be $2.1\mu F$ at 5Hz, and decreases to $10^{-4.75} \times C_0$ at 500kHz. b should be -5 if C is exactly proportional to $1/\omega$ (because $10^{-5} \times 5.0 \times 10^5 = 5$), however, it was adjusted to -4.75 by taking into consideration the eddy current effects.

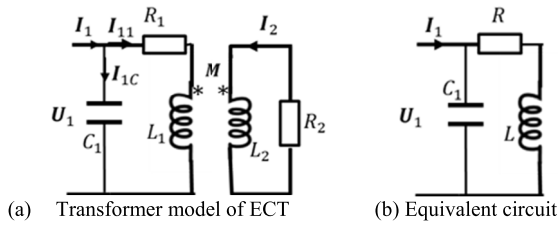


FIGURE 5. Transformer model of ECT and the equivalent circuit.

The equivalent R_{eq} , X_{eq} and L_{eq} were calculated by (3), (4) and (5). The R_{eq}/R_{dc} and L_{eq} plotted in Fig. 4(b) show that L_{eq} and R_{eq} change with frequency in a manner similar to those of measurement quantities (Fig. 3(b)), even though the values are not consistent (the stray inductance and etc. were not taken into consideration [11]). The measurement signals were qualitatively clarified.

The described numerical example confirms the theoretical analysis, demonstrates the differences between the measured resistance, reactance (inductance) and those of the coil itself. The differences and the change of differences with frequency should be taken into full consideration in coil selection, measurement condition setting and signal interpretation.

III. AIR CORED-COIL IN EDDY CURRENT TESTING

The induction coil and test material in ECT could be analogous to the primary side and the secondary side of a two-winding transformer (Fig. 5(a)): the coil itself is the primary, whereas the test object which is typically equivalent to a one-turn winding, is the secondary modelled by lumped resistance R_2 and inductance L_2 . M is mutual inductance decided by inductances L_1 , L_2 and the coupling between them, that is, $M = k\sqrt{L_1L_2}$. The coupling coefficient k ($0 < k \leq 1$) decreases when the space between the coil and the test material increases. The R_1 , L_1 and C_1 in Fig. 5(a) respectively correspond to R , L and C in Fig. 1(a).

Denoting $Z_{11} = R_1 + j\omega L_1$, $Z_M = j\omega M$, $Z_{22} = R_2 + j\omega L_2$, $Z_C = 1/j\omega C$ and following the Kirchhoff's law, we have the following equations,

$$\begin{cases} Z_{11}\dot{I}_{11} - Z_M\dot{I}_2 = \dot{U}_1 \\ \dot{I}_{1C}Z_C = \dot{U}_1 \\ Z_{22}\dot{I}_2 - Z_M\dot{I}_{11} = 0 \end{cases} \quad (12)$$

Fig. 5(b) is the equivalent circuit of Fig. 5(a), $R + j\omega L$ is equivalent to $Z_{11} - \frac{Z_M^2}{Z_{22}}$ that

$$R = R_1 + \frac{X_M^2}{R_2^2 + (\omega L_2)^2} R_2 \quad (13)$$

$$\begin{aligned} X_L &= \omega L_1 - \frac{X_M^2}{R_2^2 + (\omega L_2)^2} \omega L_2 \\ &= \omega(L_1 - \frac{X_M^2}{R_2^2 + (\omega L_2)^2} L_2) = \omega L \end{aligned} \quad (14)$$

where $X_M = \omega M$. It is obvious that $R > R_1$, whereas $L < L_1$. The rising of resistance attributes to the Joule loss in the test

material; the decreasing of inductance is owing to the fact that the magnetic flux induced by eddy currents is opposite to the flux generated by the excitation current.

With respect to the resonant properties, (7) indicates that a larger R and smaller L give rise to a smaller resonant resistance; (8) shows that a smaller L corresponds to a larger ω_0 , and consequently a higher resonant frequency ω_r . In other words, the coil with a conductive test object resonates at a frequency higher than the coil's SRF, whereas the resonant resistance is smaller than that of the coil.

The conductivity is contained in R_2 , L_2 (and M). Although the R_2 and L_2 also change with the test object's structural dimensions, we can roughly see how the R_2 and L_2 change with conductivity in terms of the surface impedance of a good conductor at high frequencies [31]

$$Z_{surface} = (1 + j)\sqrt{\frac{\omega\mu}{2\sigma}}. \quad (15)$$

Equation (15) shows that at very high frequencies that eddy currents concentrate near the surface, $R_2 = \omega L_2 = \sqrt{\omega\mu/(2\sigma)}$. For non-ferromagnetic materials that $\mu = \mu_0$, same ω/σ corresponds to same surface impedance, namely same R_2 and same L_2 . In other words, materials of different conductivities will reach the same $Z_{surface}$ at different frequencies.

IV. CONDUCTIVITY MEASUREMENT USING AN AIR-CORED COIL

The ultimate objective of this study is to detect the variation of conductivity with high sensitivity. A very straightforward approach would be extracting R_2 , L_2 (and M) from the measurement signals R_s and X_s to get the conductivity. Because the conductivity is contained in R_2 and L_2 , and appears as $\frac{Z_M^2}{Z_{22}}$ (e.g., $\frac{X_M^2}{R_2^2 + (\omega L_2)^2} R_2$ in R and $\frac{X_M^2}{R_2^2 + (\omega L_2)^2} \omega L_2$ in ωL) in the impedance viewing from the primary side, a straightforward approach to enhance detection sensitivity is to rise the ratio of $\frac{X_M^2}{R_2^2 + (\omega L_2)^2} R_2$ in R and $\frac{X_M^2}{R_2^2 + (\omega L_2)^2} \omega L_2$ in ωL . This can be achieved by reducing the impedance of the primary side, namely, using a coil of smaller R_1 and L_1 , or increasing M by having a larger coupling coefficient k , or adjusting the frequency to maximize $\frac{Z_M^2}{Z_{22}}$. No matter what the measure, the change rate of signal is generally not as large as that of conductivity, i.e., $\frac{dR_s}{R_s} < \frac{d\sigma}{\sigma}$ and $\frac{dX_s}{X_s} < \frac{d\sigma}{\sigma}$. We need to enhance the sensitivity by other means.

A. CONDUCTIVITY MEASUREMENT BY USING THE COIL IN THE INTENDED 'FREQUENCY- INVARIANT' RANGE

We might be able to improve the conductivity measurement sensitivity using certain characteristic features. Analytical solution in [9, 10] showed that in sweep frequency eddy current testing (SFECT) of equally thick conducting plates, same $\omega\sigma$ (or $f\sigma$) correspondences to same normalized impedance. Conductivity measurement base on this argument was analytically discussed in [10], followed by experimental studies. Note that the analysis in [10] were on the basis of an ideal coil,

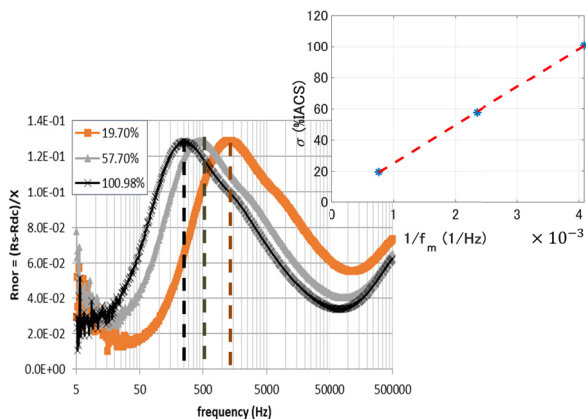


FIGURE 6. Measurement of standard test pieces' conductivity using the coil in frequency-invariant range (numbers in the legend are conductivity in IACS).

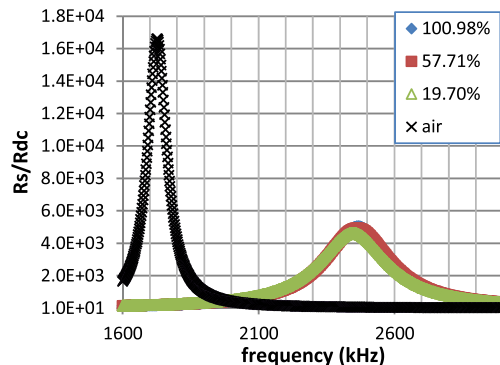
taking no consideration of a real coil's frequency properties. In this study, we re-exam this issue from the viewpoint of an actual coil's frequency characteristics.

An actual coil becomes 'ideal' over the frequency-invariant range when its DC resistance is subtracted. By the way, the impedance normalization was carried out on R_{dc} eliminated impedance signals. Thereby the derivation of ideal coil probe [9], [10] are applicable to an actual coil in its 'frequency-invariant' range. For equally thick test objects, same $\omega\sigma$ corresponds to same normalized impedance, thus same extrema, e.g., same maximum of normalized resistance, same minimum phase angle of the normalized impedance and etc. Equally thick test materials have same extrema values at same $f_m\sigma$, where f_m is the frequency of reaching extrema. Hence $\sigma \propto 1/f_m$ at the extrema points. The measurement of conductivity transforms to the measurement of frequency of reaching extrema. Because $|\frac{d\sigma}{\sigma}| \propto |-\frac{df_m}{f_m}|$, the change rate of f_m is equal to that of conductivity. And thus, the change of conductivity can be sensitively detected.

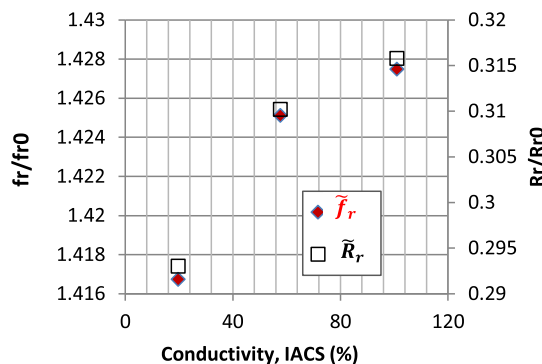
We verified the conductivity measurement on the 'same $f_m\sigma$, same impedance' principle by carrying out SFECT on three standard test pieces (TPs): 6mm thick, 50mm diameter disks of conductivities 100.98% IACS, 57.71% IACS and 19.70% IACS (Centurion NDE [29]). Fig. 6(a) shows respectively the normalized resistances' spectral. The equally thick TPs reach the same peak respectively at 1315.1Hz, 425.57Hz and 244.89Hz. The proportional relation between $1/f_m$ and σ shown in the inset of Fig. 6 demonstrates the feasibility of measuring conductivity using the 'same $f_m\sigma$, same impedance' principle.

Furthermore, we deduced the highly sensitive conductivity measuring range from the coil's frequency-invariant range. The coil is frequency-invariant from 80Hz to 80kHz as shown in Fig. (3). By extrapolating the $1/f_m \sim \sigma$ relation shown in the inset of Fig. 6, we found that the coil is able to sensitively measure conductivities ranging from 1.1% IACS to 306% IACS, on the basis of 'same $f_m\sigma$, same impedance' principle.

Note the above-mentioned method is only valid for test objects of the same thickness. This method can be applied



(a). Spectral of R_s/R_{dc} of with and without TP. (numbers in the legend are conductivity in IACS, 'air' stands for the coil in air, without a TP in vicinity).



(b) Change of \tilde{f}_r and \tilde{R}_r with conductivity

FIGURE 7. Resonant property and the relation with conductivity.

to detect conductivity change of deterioration over time that dimensional change does not occur yet. In case of 'thinning' along with degradation, the change of conductivity could be estimated from the SFECT signals' spectral in two steps: firstly estimate the thickness from the extrema value [9, 10]; secondary find out the conductivity change from the frequency of reaching the extrema by referring to the ' $1/f_m \sim \sigma$ ' of the estimated thickness. However, the ' $1/f_m \sim \sigma$ ' relation of a particular thickness might not always be available. A thickness-independent method is advisable.

B. MEASUREMENT OF CONDUCTIVITY BY USING THE COIL'S RESONANT PROPERTIES

Generally, the eddy currents penetrate into a small fraction of a test material at sufficiently high frequencies. Therefore, we seek thickness-independent conductivity measurement at high frequencies. However, because the coil's resistance and inductance are not frequency-invariant any more, same $\omega\sigma$ does not necessary render same impedance. Furthermore, the coil becomes 'capacitive' beyond the resonant frequency. Hereinafter we investigate conductivity measurement based on the coil's resonant properties.

The analysis in subsection A of Section II reveals that the change of conductivity gives rise to the change of R_2 and L_2 , and consequently change the R_r and f_r ($=\omega_r/2\pi$).

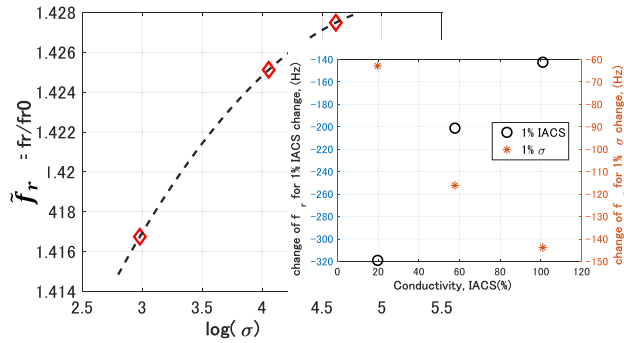


FIGURE 8. Conductivity change and the shift of resonant frequency.

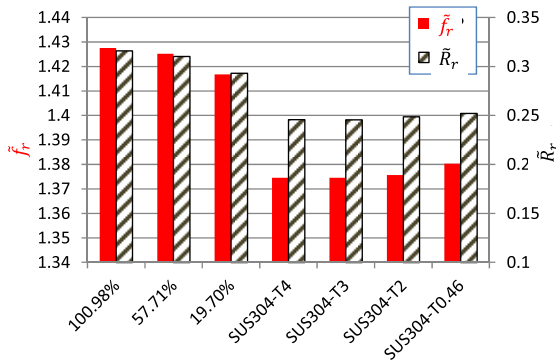


FIGURE 9. Change of characteristics resonant features, \tilde{f}_r and \tilde{R}_r with conductivity and thickness (T *: thickness in mm).

Because eddy currents distribute near the surface at resonant frequencies, the measurement of using resonant properties is expected to be less affected by the test material’s thickness.

We measured the resonant responses on the same standard TPs. Because the f_r of a coil in inspection is higher than the coil’s own SRF, the LCR meter was set to sweep from 1.6MHz to 3MHz. On the other hand, because the resonant resistance decreases when the coil is with a TP, the driven current was set to 0.09mA. Fig. 7(a) shows the spectrum of R_s of SFECT on the three TPs, along with that of without a TP (denoted as ‘air’ in Fig. 7(a)). The coil resonated respectively at 2352.5kHz, 2348.6kHz and 2334.8kHz, and the ratio R_r/R_{dc} are respectively 4511.445, 4431.689 and 4187.276. The change of f_r and R_r with conductivity shows the possibility of detecting conductivity change in terms of resonant properties. By the way, the increase of f_r with increased conductivity indirectly supports the relation stated in (15).

The ratio of resonant properties of with and without a TP were calculated by $\tilde{R}_r = \frac{R_r}{R_{r0}}$ and $\tilde{f}_r = \frac{f_r}{f_{r0}}$, and plotted against conductivity in Fig.7(b) (R_{r0} and f_{r0} are respectively the coil’s own resonant resistance and resonant frequency). The nonlinearity of relations $\tilde{R}_r \sim \sigma$ and $\tilde{f}_r \sim \sigma$ implies that the measurement sensitivity changes over the range. Here we investigated the sensitivity in terms of $\tilde{f}_r \sim \sigma$ relation. Fig. 8 shows a 2nd order polynomial fitting of $\log(\sigma) \sim \tilde{f}_r$. The changes of $f_r (= \tilde{f}_r \times f_{r0})$ with respect to 1%IACS conductivity increment and 1% σ conductivity increment were calculated

based on the fitting. The inset of Fig. 8 shows that 1%IACS conductivity increment of 19.8% IACS, 57.71% IACS and 100.98% IACS materials respectively causes 319Hz, 201Hz and 142Hz decrement of f_r . Whereas the f_r respectively decreases 143Hz, 116Hz and 63Hz for 1% σ conductivity increment. The change of conductivity results in a shift of f_r . We will be able to detect slight conductivity variation by means of fine frequency adjustment.

For field applications, we need to know to what extent the measurement is thickness independent. We implemented the same SFECT measurement on 4mm, 3mm, 2mm and 0.46mm thick SUS304 plates and obtained the \tilde{f}_r and \tilde{R}_r , respectively. Fig. 9 shows that the measurement quantities of 4mm and 3mm thick TPs are almost identical, but slightly different from those of 2mm thick TP. The \tilde{f}_r of the 0.46mm thick TP is notably different from that of the others. The results tell us that the coil is able to detect conductivity change of 3mm or even thicker SUS304 plates regardless of thickness. For thinner TPs, however, the effect of thickness cannot be completely neglected. The results suggested that we should know a coil’s limit on measurable thickness in using a coil’s resonant properties. Proper coil design and selection are required.

V. CONCLUSION

We investigated an air-cored coil’s frequency properties and found that what we measured, the equivalent resistance and inductance, are not consistent with those of the coil itself at all frequencies. At very low frequencies, the equivalent resistance is almost equal to, whereas the equivalent inductance is smaller than that of the coil. In the conventional ECT frequency range, the equivalent resistance and inductance are frequency-invariant, being almost equal to those of the coil. At high frequencies, the equivalent ones increase sharply and the coil resonates at its SRF. The coil and the test object in ECT were modelled as a two-winding transformer. The equivalent resistance and inductance change with the test object.

For equally thick test pieces, the change of conductivity could be sensitively measured using the coil’s ‘frequency-invariant’ properties on the basis of the ‘same $\omega\sigma$, same impedance’ principle. The measurement of conductivity was transformed to the measurement of frequency of reaching normalized impedance’s extrema. In addition, the range of conductivity that a coil can sensitively and accurately measure could be deduced from the coil’s frequency-invariant range.

The coil’s resonant properties were also applied to detect conductivity change independently on thickness. The coil resonates at higher frequencies and the resonant resistance is smaller when the coil is in inspection. Change of conductivity could be sensitively perceived from the shift of resonant frequency or change of resonant resistance. Slight variation on conductivity can be detected by fine frequency adjustment.

This study therefore indicates that a probe coil should be utilized in accordance with its frequency characteristics.

REFERENCES

- [1] *Nondestructive Testing Handbook*, vol. 4, 2nd ed., Electromagn. Test., Amer. Soc. Nondestruct. Test., Columbus, OH, USA, 1986.
- [2] J. Blitz, *Electrical and Magnetic Methods of Nondestructive Testing*. Bristol, U.K.: IOP Publishing, 1991.
- [3] T. P. Theodoulidis and E. E. Kriezis, *Eddy Current Canonical Problems (With Applications to Nondestructive Evaluation)*, 1st ed. Henderson, NV, USA: Tech Science Press, 2006.
- [4] C. C. Cheng, C. V. Dodd, and W. E. Deeds, "General analysis for probe coils near stratified conductors," *Int. J. NDT*, vol. 3, pp. 109–130, 1971.
- [5] Y. Kraftmakher, "Eddy currents: Contactless measurement of electrical resistivity," *Amer. J. Phys.*, vol. 68, no. 4, pp. 375–379, Apr. 2000, doi: 10.1119/1.19440.
- [6] C. Wang, M. Fan, B. Cao, B. Ye, and W. Li, "Novel noncontact eddy current measurement of electrical conductivity," *IEEE Sensors J.*, vol. 18, no. 22, pp. 9352–9359, Nov. 2018.
- [7] J. Ñiguez, V. Raposo, and M. Zazo, "Measurement of electrical conductivity in nonferromagnetic tubes and rods at low frequencies," *Amer. J. Phys.*, vol. 77, no. 10, pp. 949–953, Oct. 2009, doi: 10.1119/1.3184154.
- [8] J. Ñiguez, V. Raposo, A. G. Flores, M. Zazo, and A. Hernández-López, "Measurement of the electrical conductivity of metallic tubes by studying magnetic screening at low frequency," *Amer. J. Phys.*, vol. 73, no. 3, pp. 206–210, Mar. 2005, doi: 10.1119/1.1842730.
- [9] W. Cheng, "Thickness measurement of metal plates using swept-frequency eddy current testing and impedance normalization," *IEEE Sensors J.*, vol. 17, no. 14, pp. 4558–4569, Jul. 2017.
- [10] W. Cheng, "Swept-frequency eddy current testing to characterize a non-magnetic metallic plate and a nonconductive coating over it," *Int. J. Appl. Electromagn. Mech.*, vol. 59, no. 3, pp. 1169–1178, Mar. 2019.
- [11] R. Feynman, B. R. Leighton, and M. Sands, "AC circuit, and 'cavity resonator,'" in *The Feynman Lectures on Physics*, vol. 2. Reading, MA, USA: Addison-Wesley, 1964.
- [12] M. Cacciola, S. Calcagno, G. Megali, D. Pellicanó, M. Versaci, and F. C. Morabito, "Eddy current modeling in composite materials," *PIERS Online*, vol. 5, no. 6, pp. 591–595, 2009.
- [13] C. Beine, C. Boller, U. Netzelmann, F. Porsch, R. Venkat, M. Schulze, A. Bulavinov, and H. Heuer, "NDT for CFRP aeronautical components a comparative study," in *Proc. 2nd Int. Symp. NDT Aerosp.*, 2010, pp. 1–9.
- [14] H. Heuer, M. H. Schulze, and N. Meyendorf, "High resolution inspection of carbon fiber materials by eddy current techniques," in *Proc. 2nd Int. Symp. NDT Aerosp.*, 2010, pp. 1–13.
- [15] K. Koyama and H. Hoshikawa, "Detection of damage in carbon fiber-reinforced plastics (CFRP) by eddy current testing," (in Japanese), *J. Non-destruct. Inspection*, vol. 60, no. 9, pp. 536–540, 2011.
- [16] K. Tsukada, Y. Haga, K. Morita, N. Song, K. Sakai, T. Kiwa, and W. Cheng, "Detection of inner corrosion of steel construction using magnetic resistance sensor and magnetic spectroscopy analysis," *IEEE Trans. Magn.*, vol. 52, no. 7, pp. 1–4, Jul. 2016.
- [17] W. Cheng and I. Komura, "Optimum inducement of eddy current for NDE of deep lying defects: An analytical approach," *Int. J. Appl. Electromagn. Mech.*, vol. 33, nos. 1–2, pp. 377–385, Oct. 2010.
- [18] W. Cheng, "Electromagnetic nondestructive evaluation of defects in ferromagnetic structures," *AIP Conf.*, vol. 1806, no. 1, 2017, Art. no. 110024, doi: 10.1063/1.4974702.
- [19] M. Shiwa, W. Cheng, S. Nakahigasi, and I. Komura, "Nondestructive evaluation of irradiation embrittlement of SQV2A steel by using magnetic method," in *Proc. Rev. Quant. Nondestruct. Eval.*, vol. 25, 2005, pp. 1163–1170.
- [20] X. Chen and Y. Lei, "Electrical conductivity measurement of ferromagnetic metallic materials using pulsed eddy current method," *NDT & E Int.*, vol. 75, pp. 33–38, Oct. 2015.
- [21] E. A. Pfeif, Z. Jones, A. N. Lasseigne, K. Koenig, K. Krzywosz, E. V. Mader, S. Yagnik, B. Mishra, and D. L. Olson, "Submerged eddy current method of hydrogen content evaluation of zircaloy-4 fuel cladding," *Rev. Prog. Quant. Nondestruct. Eval.*, vol. 1335, pp. 1168–1175, Jun. 2011, doi: 10.1063/1.3592067.
- [22] M. P. Blodgett and P. B. Nagy, "Eddy current assessment of near-surface residual stress in shot-peened nickel-base superalloys," *J. Nondestruct. Eval.*, vol. 23, no. 3, pp. 107–123, Sep. 2004.
- [23] B. A. Abu-Nabah and P. B. Nagy, "High-frequency eddy current conductivity spectroscopy for residual stress profiling in surface-treated nickel-base superalloys," *NDT & E Int.*, vol. 40, no. 5, pp. 405–418, Jul. 2007.
- [24] G. Sposito, C. Ward, P. Cawley, P. B. Nagy, and C. Scruby, "A review of non-destructive techniques for the detection of creep damage in power plant steels," *NDT & E Int.*, vol. 43, no. 7, pp. 555–567, Oct. 2010.
- [25] K. Mohri, *Science and Engineering of Magnetic Sensor: From Principle to Application*. Corona, (in Japanese), 2015.
- [26] H. A. Wheeler, "Simple inductance formulas for radio coils," *Proc. Inst. Radio Eng.*, vol. 16, no. 10, pp. 1398–1400, 1928, doi: 10.1109/JRPROC.1928.221309.
- [27] MATLAB. Accessed: Sep. 10, 2020. [Online]. Available: <https://jp.mathworks.com/help/matlab/ref/logspace.html>
- [28] *User's Manual of IM3536 LCR Meter*, (in Japanese), 2nd ed., HIOKI, Nagano, Japan, Sep. 2016.
- [29] *The Homepage of Centurion NDT*. Accessed: Sep. 10, 2020. [Online]. Available: <https://www.centurionndt.com/conductivity.html>
- [30] M. B. Heaney, *Electrical Conductivity and Resistivity, Electrical Instrument, Signal Processing, and Displays*, J. G. Webster, Ed. Boca Raton, FL, USA: CRC Press, 2003.
- [31] D. M. Pozar, "Electromagnetic theory," in *Microwave Engineering*, 4th ed. Hoboken, NJ, USA: Wiley, 2011.



WEIYING CHENG received the B.S. and M.S. degrees in electrical engineering from Zhejiang University, Hangzhou, China, in 1988 and 1991, respectively, and the Ph.D. degree in quantum engineering and systems science from The University of Tokyo, Tokyo, Japan, in 2000.

From 1991 to 1996, she was a Lecturer with the Department of Electrical Engineering, Zhejiang University. From 2000 to 2002, she was a Researcher with the Science Solutions International Laboratory, Tokyo. Since 2002, she has been a Principal Researcher with the NDE Center, Japan Power Engineering and Inspection Corporation, Yokohama, Japan. Her research interests include numerical modeling and simulation, data analysis and signal processing, and nondestructive testing and evaluation.

Dr. Cheng is a member of the Institute of Electrical Engineering of Japan, the Japan Society of Non-Destructive Inspection, and the Japan Society of Maintenance.

• • •